

## DYNAMICAL INTERACTIONS OF PLANETARY SYSTEMS IN DENSE STELLAR ENVIRONMENTS

JOHN M. FREGEAU<sup>1</sup>, SOURAV CHATTERJEE<sup>2</sup>, & FREDERIC A. RASIO<sup>3</sup>  
Department of Physics and Astronomy, Northwestern University, Evanston, IL 60208  
*Accepted for publication in ApJ*

### ABSTRACT

We study dynamical interactions of star–planet binaries with other single stars. We derive analytical cross sections for all possible outcomes, and confirm them with numerical scattering experiments. We find that a wide mass ratio in the binary introduces a region in parameter space that is inaccessible to comparable-mass systems, in which the nature of the dynamical interaction is fundamentally different from what has traditionally been considered in the literature on binary scattering. We study the properties of the planetary systems that result from the scattering interactions for all regions of parameter space, paying particular attention to the location of the “hard–soft” boundary. The structure of the parameter space turns out to be significantly richer than a simple statement of the location of the “hard–soft” boundary would imply. We consider the implications of our findings, calculating characteristic lifetimes for planetary systems in dense stellar environments, and applying the results to previous analytical studies, as well as past and future observations. Recognizing that the system PSR B1620-26 in the globular cluster M4 lies in the “new” region of parameter space, we perform a detailed analysis quantifying the likelihood of different scenarios in forming the system we see today.

*Subject headings:* stellar dynamics — planetary systems — globular clusters: general — methods:  $n$ -body simulations — pulsars: individual (1620-26)

### 1. INTRODUCTION

The subject of planets in dense stellar systems such as globular clusters came to life with the discovery that the binary pulsar PSR B1620-26 in the globular cluster M4 is orbited by a distant companion of approximately Jupiter mass (Backer 1993; Thorsett et al. 1999; Sigurdsson et al. 2003, and references therein). The presence of such a system near the core of M4 is, at first, puzzling for several reasons. For example, the metallicity of M4 is low ( $0.05Z_{\odot}$ ), making the formation of such a planet via the standard core accretion model very unlikely, and sparking the creation of alternative formation theories (Beer et al. 2004, and references therein). In addition, the planet is on such a wide orbit about its host that the system should have been destroyed by dynamical interactions on a very short timescale ( $\sim 10^8$  yr) in the moderately high density environment of M4’s core, implying that it must have been formed recently via an alternative mechanism such as a dynamical interaction involving a binary.

Campaigns searching for “hot Jupiter” planets (with orbital periods  $\lesssim 10$  d) in 47 Tuc have yielded null detections, instead placing upper limits on the hot Jupiter frequency there (Gilliland et al. 2000; Wel Drake et al. 2005). It now appears that the lack of hot Jupiters detected in 47 Tuc is probably more closely connected with the low metallicity of the environment, and not simply due to destruction via dynamical encounters in the high density stellar environment. This result is consistent with the strong correlation between host star metallicity and planet frequency in observed systems (Fischer & Valenti 2005). Searches for planets via transits in the higher metallicity environments of open clus-

ters are currently underway<sup>4</sup>.

A key ingredient in the formation and evolution of planetary systems in dense stellar environments that is absent in lower density environments is dynamics. If either the stellar density is large enough or the planetary system is wide enough, it is likely to undergo a strong dynamical scattering interaction with another star or binary, perturbing its properties or possibly destroying it in the process. The importance of dynamics for wide mass ratio binaries cannot be overstated, especially when one considers the wealth of low-mass objects such as brown dwarfs that are known to exist in open and globular clusters, and may be in binaries. In addition, the importance of dynamics as early as the stage of star formation is now becoming clear. There is now convincing evidence that a distant encounter with another star is responsible for the currently observed properties of distant Solar System objects such as Sedna (Kenyon & Bromley 2004; Morbidelli & Levison 2004; Kobayashi et al. 2005). The object HD 188753 is a hierarchical triple star system composed of a main-sequence star in an  $\approx 12.3$  AU orbit about a compact main-sequence binary. What makes this system interesting is that the single star hosts a hot Jupiter in orbit about it, with a semimajor axis of  $\approx 0.04$  AU (Konacki 2005). The current configuration of the system is puzzling, since the binary companion would truncate the initial disk out of which the planet could have formed at a radius much smaller than that required by either the core accretion or gravitational fragmentation paradigms. It is now clear that the current configuration of HD 188753 must have resulted from a dynamical scattering interaction in a moderately dense stellar environment (Pfahl 2005; Portegies Zwart & McMillan 2005).

The types of dynamical interactions we have been

<sup>1</sup> fregeau@alum.mit.edu

<sup>2</sup> s-chatterjee@northwestern.edu

<sup>3</sup> rasio@northwestern.edu

<sup>4</sup> see <http://star-www.st-and.ac.uk/~kdh1/transits/table.html>

discussing have been studied in great detail and volume since at least the mid-1970s for the case of comparable masses (Hills 1975; Heggie 1975; Heggie & Hut 2003, and references therein). The case of disparate masses in the binary (such as for a planetary system) has been treated in less detail (Hills 1984; Hills & Dissly 1989; Sigurdsson 1992), but with considerable attention paid to the survivability of planetary systems in particular (Laughlin & Adams 1998; Bonnell et al. 2001; Davies & Sigurdsson 2001). To the best of our knowledge, there has not yet been a comprehensive treatment of dynamical scattering interactions with wide mass ratio systems in the literature, as previous work has typically been concerned with a numerical treatment of a certain aspect of the problem. This paper is an attempt to remedy this situation by carefully treating a wide range of parameter space both analytically and numerically, and identifying physically distinct regions of the space, with an emphasis on application to physically interesting problems.

In particular, the questions we would like to answer in this paper are the following: for a dynamical interaction between a star–planet system and another star, under what conditions does the interaction result in: 1) preservation of the planetary system, in the sense that the planet remains in orbit about its parent star, even if the orbit is perturbed; 2) exchange of the incoming star for the planetary system’s host star; 3) destruction of the planetary system, in the sense that the planet is not bound to either star after the interaction; and 4) physical collisions involving two or more of the three objects? For the outcome in question 2, we would also like to know the resulting properties of the planetary system’s orbit. In particular, we would like to know the regimes in which the planetary system orbit shrinks and those in which it widens.

In the language of binary scattering, the interaction of a binary planetary system with a single star can be written symbolically as  $[M_1 m] M_2$ , where the  $M_i$  represent the stars, and  $m$  represents the planet. The possible outcomes can be enumerated succinctly as shown in Table 1. The outcome “pres” is preservation of the planetary system, and can result either from a strong interaction or a weak fly-by. The planetary system can have shrunk or widened in the process. The outcome “ex\_s” is an exchange in which the host star of the planetary system is exchanged for the incoming star. The outcome “ex\_p” is an exchange in which the two stars remain bound, ejecting the planet. The outcome “ion” leaves all objects (stars and planet) unbound from each other. The remaining outcomes listed in the table are various permutations involving one or more collisions. The outcome of a stable hierarchical triple is omitted from the table since it is classically forbidden (Heggie & Hut 2003). It is possible to be formed as a result of a binary–single interaction if tidal effects are present. However, we ignore such effects in this paper.

Clearly, case 1 above corresponds to outcome “pres”, case 2 corresponds to outcome “ex\_s”, and case 3 corresponds to outcomes “ex\_p” and “ion”. The outcomes corresponding to case 4 are the remaining listed in the table. In this paper we address the questions posed above by calculating cross sections for the processes listed, as well as characteristic lifetimes. In section 2 we treat as

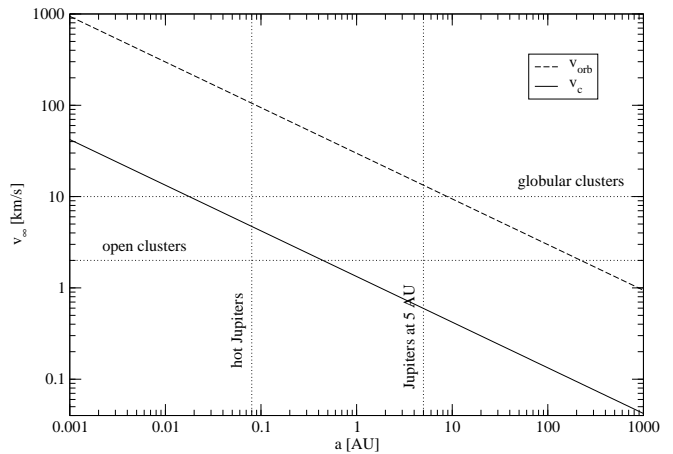


FIG. 1.— Plot of the critical velocity  $v_c$  and orbital speed  $v_{\text{orb}}$  for a planetary system composed of a  $1M_{\odot}$  star and a  $10^{-3}M_{\odot}$  planet in an orbit with semimajor axis  $a$ , encountering a  $1M_{\odot}$  star with relative velocity at infinity  $v_{\infty}$ . Dotted lines represent characteristic velocity dispersions for open and globular clusters, and orbital sizes for hot Jupiters and Jupiters at 5 AU, as shown.

much of the problem as we can analytically. In section 3 we confirm our analytical predictions with numerical experiments. In section 4 we determine under what conditions the planetary system will shrink or expand as the result of an exchange encounter, and the average amount by which it shrinks or expands. In section 5 we discuss the implications of the results in the context of current literature and observations. In section 6 we quantify the likelihood of the possible dynamical formation scenarios of the planetary system PSR B1620-26 in the globular cluster M4. Finally, in section 7 we summarize and conclude.

## 2. ANALYTICAL CONSIDERATIONS

As described above, we symbolically label the interaction between a planetary system and a single star as  $[M_1 m] M_2$ . We also use the symbols  $M_i$  and  $m$  for the masses of the bodies, along with  $a$  for the planetary system semimajor axis,  $e$  for its eccentricity,  $v_{\infty}$  for the relative velocity at infinity between the planetary system and single star, and  $b$  for the impact parameter. If one treats all bodies as point particles, and only considers their masses for the time being, there are only two velocity scales in the problem. The first is what has historically been called the critical velocity, which is the value of  $v_{\infty}$  for which the total energy of the binary–single system is zero, and is given by

$$v_c = \left( \frac{GM_1 m}{\mu a} \right)^{1/2}, \quad (1)$$

where  $\mu = (M_1 + m)M_2/(M_1 + M_2 + m)$  is the reduced mass of the binary–single star system. The second is the orbital speed of the planet relative to its parent star, and is given by

$$v_{\text{orb}} = \sqrt{\frac{G(M_1 + m)}{a}}, \quad (2)$$

for a circular orbit. Looking at eqs. (1) and (2), we see that if all the masses in the problem are comparable, then  $v_c \approx v_{\text{orb}}$ . If, on the other hand, one of the members of

TABLE 1  
POSSIBLE OUTCOMES OF A DYNAMICAL SCATTERING INTERACTION BETWEEN A  
PLANETARY SYSTEM, ‘ $[M_1 m]$ ’, AND A SINGLE STAR, ‘ $M_2$ ’.

outcome	description	nickname
$[M_1 m] M_2$	preservation	“pres”
$[M_2 m] M_1$	exchange host star for incoming star	“ex_s”
$[M_1 M_2] m$	exchange planet for incoming star	“ex_p”
$M_1 M_2 m$	ionization	“ion”
$[M_i:m M_j]$	collision of planet with one star, resulting in binary	
$M_i:m M_j$	collision of planet with one star, resulting in ionization	
$[M_i:M_j m]$	collision of two stars, resulting in binary	
$M_i:M_j m$	collision of two stars, resulting in ionization	
$M_i:M_j:m$	collision of all objects	

NOTE. — The symbol ‘:’ denotes a physical collision.

the binary system is much less massive than the other member (as is the case for a planetary system), and we take  $M_1 = M_2 \equiv M$ , and  $q \equiv m/M \ll 1$ , then we can approximately write  $v_c \approx \sqrt{q}v_{\text{orb}}$ . For a typical planetary system,  $q \sim 10^{-3}$ , and the two velocities differ by more than an order of magnitude. Fig. 1 plots the two velocities for a planetary system with  $q = 10^{-3}$  and  $M = M_\odot$  as a function of  $a$ . In essence, introducing a mass ratio in the binary opens up a strip in parameter space (between the two lines in Fig. 1) in which the physical character of dynamical scattering interactions is fundamentally different from that of the comparable-mass case.

In the literature on binary scattering involving stars of comparable mass,  $v_c$  is the velocity delimiting the border between “hard” and “soft” binaries (Heggie 1975). If  $v_\infty < v_c$ , the binary is in the hard regime, and will on average harden ( $a$  will get smaller) as a result of an encounter. On the other hand, if  $v_\infty > v_c$ , the binary is in the soft regime, and will on average soften ( $a$  will get larger) as a result of an encounter—that is, if the binary is not destroyed completely. However, Hills & Dissly (1989) and Hills (1990) suggest that when considering binaries with disparate masses, the boundary is more accurately given by  $v_\infty = v_{\text{orb}}$ , and not by  $v_\infty = v_c$ , and suggest the use of the terminology “fast–slow boundary” rather than “hard–soft boundary”, since it is the relative speed of the binary members that is physically relevant. In the literature considering the survivability of planetary systems (and high mass ratio systems in general) in dense stellar environments, both  $v_c$  and  $v_{\text{orb}}$  have been used as the single characteristic velocity delimiting the boundary between ionization on the high-velocity side and hardening on the low-velocity side. However, as we will see below, for planetary systems the hard–soft boundary lies at  $v_\infty = v_c$ , while the characteristic timescale for the survivability of a planetary system in a dense environment drops markedly only at  $v_\infty = v_{\text{orb}}$ .

Having written down the two characteristic velocities in the problem, thus dividing parameter space into three distinct regions (as shown in Figure 1), the question naturally arises: What is the physical character of the scattering interactions in each of the three regions? For  $v_\infty < v_c$ , the total energy of the binary–single system is negative. We thus expect that for any “strong” encounter (defined approximately as one in which the classical pericenter distance,  $r_p$ , between the single star and the planetary system is of order  $a$ ), the interaction will be

resonant, in the sense that it will survive for many orbital times (Heggie & Hut 2003). It will behave as a small star cluster, most likely ejecting its lightest member—in this case the planet—yielding the outcome “ex\_p (res)”. For  $r_p \gtrsim a$ , the likely outcome is a “direct” exchange of the incoming star for the planet (“ex\_s”). We thus expect  $\sigma_{\text{ex-p}} = \sigma_{\text{ex-p(res)}} + \sigma_{\text{ex-p(non-res)}}$  to be the dominant cross section for  $v_\infty < v_c$ . For  $v_\infty > v_{\text{orb}}$ , the interaction is impulsive, since the timescale of the interaction is a small fraction of the binary orbital period. We thus expect that any “strong” interaction will ionize the system, making  $\sigma_{\text{ion}}$  the dominant cross section in this regime. For  $v_c < v_\infty < v_{\text{orb}}$  the timescale of the interaction is comparable to the orbital period, so the outcome is not a priori obvious, and must be treated numerically.

Below, as far as it is possible, we calculate using analytical techniques the cross sections for each outcome in each of the three regions of parameter space.

### 2.1. $v_\infty < v_c$

First, since for  $v_\infty < v_c$  the total energy of the binary–single system is negative, it is clear that ionization is classically forbidden. Thus

$$\sigma_{\text{ion}} = 0. \quad (3)$$

We should also mention that for the outcome of preservation the only method we have for determining if an interaction was “strong” is whether or not it was resonant. Thus it should be clear that for every region of parameter space in Figure 1

$$\sigma_{\text{pres(non-res)}} \rightarrow \infty, \quad (4)$$

since every very distant passage of the single star by the binary preserves it via a non-resonant interaction.

Heggie et al. (1996) considered interactions of “hard” binaries (in the sense that  $v_\infty < v_c$ ) with single stars for a wide range of possible mass ratios in the binary and between the binary members and the incoming single star. Using analytical techniques, they calculated the scaling of the cross sections for each possible outcome. They then fit to numerically calculated cross sections to determine the weakly mass-dependent “coefficients” on each cross section. From their eqs. (13) and (14) with  $m_2 \approx m_3$  (since  $M_1 \approx M_2$  here), we see that

$$\sigma_{\text{ex-p(res)}} \approx \sigma_{\text{ex-p(non-res)}}. \quad (5)$$

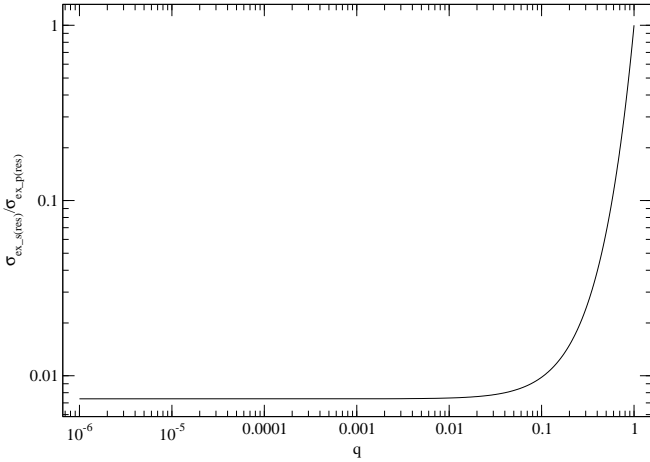


FIG. 2.— Plot of the ratio of the cross section for resonant exchange in which the planet’s original host star is ejected, to that in which the planet is ejected,  $\sigma_{\text{ex-s(res)}}/\sigma_{\text{ex-p(res)}}$ , as a function of the binary mass ratio  $q \equiv m/M$ . Here we have assumed that both stars have mass  $M$ . Note how, as  $q$  is decreased from unity, the test-particle limit is reached relatively quickly, at  $q \approx 0.1$ .

The cross section for non-resonant exchange of the planet for the incoming star is given by their eq. (17) (divided by 2 since  $\sigma_{\text{ex-p(res)}} \approx \sigma_{\text{ex-p(non-res)}}$ ):

$$\begin{aligned} \sigma_{\text{ex-p(non-res)}} &\approx \frac{\pi G M_t a}{4v_\infty^2} \left( \frac{M_1 + M_2}{M_t} \right)^{1/6} \\ &\times \left( \frac{M_2}{m + M_2} \right)^{7/2} \left( \frac{M_1 + m}{M_t} \right)^{-1/3} \left( \frac{M_2 + m}{M_t} \right) \\ &\times \exp \left( \sum_{m,n} a_{mn} \left( \frac{m}{M_1 + m} \right)^m \left( \frac{M_2}{M_t} \right)^n \right), \quad (6) \end{aligned}$$

where  $M_t = M_1 + m + M_2$  is the total mass of the binary–single system, the exponential term is the “coefficient” fit to the numerical results, and the  $a_{mn}$  are given in their Table 3.

The cross section for direct exchange of the incoming star for the host star is also given by their eq. (17), with the appropriate permutation of masses:

$$\begin{aligned} \sigma_{\text{ex-s(non-res)}} &\approx \frac{\pi G M_t a}{2v_\infty^2} \left( \frac{M_2 + m}{M_t} \right)^{1/6} \\ &\times \left( \frac{M_2}{M_1 + M_2} \right)^{7/2} \left( \frac{M_1 + m}{M_t} \right)^{-1/3} \left( \frac{M_1 + M_2}{M_t} \right) \\ &\times \exp \left( \sum_{m,n} a_{mn} \left( \frac{M_1}{M_1 + m} \right)^m \left( \frac{M_2}{M_t} \right)^n \right). \quad (7) \end{aligned}$$

The resonant cross section for this process,  $\sigma_{\text{ex-s(res)}}$ , can be calculated approximately by statistical techniques. Since for a resonant interaction we expect the three-body system to behave like a small star cluster, we can assume that the less massive body (the planet) and the more massive bodies (the stars) reach energy equipartition, yielding the approximate equality

$$mv_{\sigma,m}^2 = Mv_{\sigma,M}^2, \quad (8)$$

where  $v_{\sigma,m}$  is the one-dimensional velocity “dispersion” of the planet,  $v_{\sigma,M}$  is the one-dimensional velocity dispersion of the stars, and we let  $M_1 = M_2 = M$ . Assuming that the three body system reaches thermal equilibrium on a timescale shorter than the interaction timescale, each species obeys a Maxwellian distribution:

$$f(v, n, v_\sigma) = 4\pi v^2 \frac{n}{(2\pi v_\sigma^2)^{3/2}} e^{-v^2/2v_\sigma^2}, \quad (9)$$

where  $n$  is the number density of the species,  $v_\sigma$  its one-dimensional velocity dispersion, and  $v$  its speed. To find the ratio of the probability for ejecting one of the stars to ejecting the planet, one simply integrates the velocity distribution for each species from the escape velocity,  $v_{\text{esc}}$ , to infinity and considers the ratio. Using the fact that  $v_{\text{esc}} \approx 2\sqrt{3}v_\sigma$ , where  $v_\sigma \approx v_{\sigma,M}$  is the one-dimensional velocity dispersion of the full three-object system, we have

$$\begin{aligned} \frac{\sigma_{\text{ex-s(res)}}}{\sigma_{\text{ex-p(res)}}} &= \frac{\int_{2\sqrt{3}v_\sigma}^{\infty} f(v, n, v_\sigma) dv}{\int_{2\sqrt{3}v_\sigma}^{\infty} f(v, n, v_\sigma/\sqrt{q}) dv} \\ &= \frac{2e^{-6} \sqrt{\frac{6}{\pi}} + \text{erfc}(\sqrt{6})}{2e^{-6q} \sqrt{\frac{6q}{\pi}} + \text{erfc}(\sqrt{6q})}, \quad (10) \end{aligned}$$

where  $\text{erfc}(z) = 1 - \text{erf}(z)$  is the complement of the error function. Note that there is no factor of two in the numerator since the two stars in the system are distinguishable, in the sense that we distinguish between “ex-s(res)” and “pres(res)”. This function is plotted in Fig. 2. Note how, as  $q$  is decreased from unity, the test particle limit is reached relatively quickly, at  $q \approx 0.1$ . The same qualitative result is found in Fregeau et al. (2004), as shown in their Figure 10.

Since in a resonant interaction the system loses all memory of its initial configuration, we expect that for  $M_1 = M_2 = M$ , the probability of preserving the system (and ejecting the incoming star) in a resonant interaction is equal to that of ejecting the host star and keeping the incoming star:

$$\sigma_{\text{pres(res)}} = \sigma_{\text{ex-s(res)}}. \quad (11)$$

Finally, we remark on the likelihood of collisions in this regime. Fregeau et al. (2004) have studied in detail the probability of collisions during binary interactions, including binaries with very small mass ratios, and found that for systems in which the radius of the low-mass member is independent of its mass (as is approximately the case for planets), the test particle limit is reached at  $q \approx 0.1$  (see Figure 10 of that paper). In other words, the collision cross section is independent of the mass of the low-mass member below  $q \approx 0.1$ . Furthermore, the collision cross section is roughly as large as the strong interaction cross section. Therefore, we expect the combined cross section for any outcome involving a collision to be on the same order as  $\sigma_{\text{ex-p(res)}}$ . This estimate says nothing about the relative frequency of the different outcomes involving collisions, which requires numerical calculations to infer, and which we do not treat in this paper. However, we do consider collisions briefly in the discussion of PSR B1620-26 in section 6.

In the regime  $v_\infty > v_{\text{orb}}$ , since  $v_\infty > v_c$ , the total energy of the system is positive, so resonant scattering is forbidden:

$$\sigma_{\text{pres(res)}} = \sigma_{\text{ex-s(res)}} = \sigma_{\text{ex-p(res)}} = 0. \quad (12)$$

Since  $v_\infty > v_{\text{orb}}$ , the timescale of the scattering interaction is typically much smaller than the orbital period (unless  $r_p \gg a$ ). In this case the interaction is in the impulsive limit, and can be handled quite efficiently with analytical techniques (Hut 1983). From eq. (5.1') of Hut (1983), the ionization cross section is

$$\sigma_{\text{ion}} = \frac{40}{3} \pi a G \frac{M_2^2}{M_1 + m} \frac{1}{v_\infty^2}. \quad (13)$$

Exchange in the impulsive regime occurs when the incoming star,  $M_2$ , passes much closer to one member of the binary than the other, and undergoes a near-180° encounter in which all of its momentum is transferred to that member. In order for  $M_2$  to remain bound in the binary, it must receive nearly zero recoil in the frame of the remaining binary member, requiring that the mass of  $M_2$  be nearly equal to the mass of the binary member it displaces (Hut 1983). Thus exchange of the planet for the incoming star,  $\sigma_{\text{ex-p(non-res)}}$ , is vanishingly small unless  $M_2 \approx m$ . Exchange of the planet's host star for the incoming star, on the other hand, is more likely since the stars' masses are more likely to be comparable. From eq. (5.2') of Hut (1983), the cross section for exchange of the planet's host star for the incoming star is given by

$$\sigma_{\text{ex-s(non-res)}} = \frac{20}{3} \pi \frac{1}{a} G^3 M^2 (M + m) \frac{1}{v_\infty^6}, \quad (14)$$

with  $M_1 = M_2 = M$ .

### 2.3. $v_c < v_\infty < v_{\text{orb}}$

In the regime  $v_c < v_\infty < v_{\text{orb}}$ , the interaction is neither resonant nor impulsive, so the techniques used above cannot be used here. For  $q \ll 1$  the interaction is essentially the hyperbolic restricted three-body problem, but since the timescale of the interaction is of order a few orbital periods, the standard techniques of perturbation theory are of limited use. Instead, one must appeal to numerical methods to discern the nature of the interactions. It is possible, however, to make order of magnitude estimates of the relevant cross sections. Whenever  $M_2$  passes within  $r_p \lesssim a$  of the binary, its force on the planet is comparable to that of  $M_1$ , in which case the orbit of the planet should be sufficiently perturbed so as to unbind it from the host star and either eject it from the system or leave it bound to  $M_2$ . Thus we estimate that the total cross section  $\sigma_{\text{ion}} + \sigma_{\text{ex-s(non-res)}}$  should be roughly equal to the strong interaction cross section. In the absence of any more detailed information, we simply assume  $\sigma_{\text{ion}} \approx \sigma_{\text{ex-s(non-res)}}$ , yielding

$$\sigma_{\text{ion}} \sim \sigma_{\text{ex-s(non-res)}} \sim \pi a \frac{GM_t}{v_\infty^2}, \quad (15)$$

since gravitational focusing dominates. Since in this regime the planet is effectively a test particle,  $\sigma_{\text{ex-p(non-res)}}$  is vanishingly small.

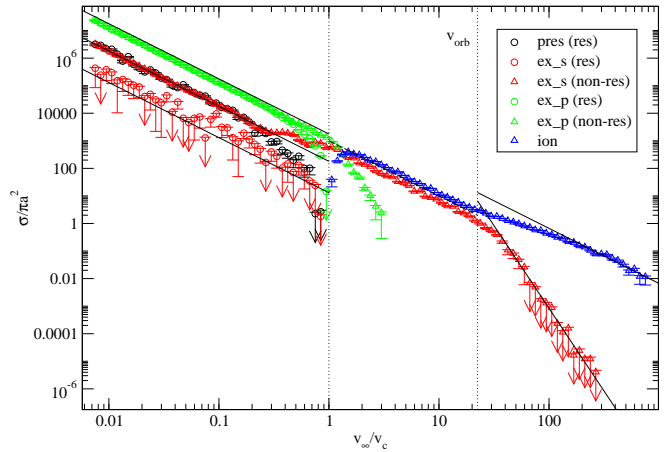


FIG. 3.— The dimensionless cross sections,  $\sigma/\pi a^2$ , for the outcomes involving no collisions in Table 1, as a function of  $v_\infty/v_c$  for scattering interactions between a planetary system with mass ratio  $q = m/M = 10^{-3}$  and eccentricity  $e = 0$ , and a star of mass  $M$ . Points plotted are as described in the legend. Circles represent resonant interactions, while triangles represent non-resonances (“direct” interactions). The error bars plotted are one-sigma. The vertical dotted lines are the critical velocity and orbital speed. The solid lines are the analytically predicted cross sections from section 2, while the dashed line is the order of magnitude estimated cross section from the same section.

### 3. NUMERICAL CONFIRMATION

To confirm the analytical predictions of the previous section, we have calculated the cross sections by numerically integrating many scattering interactions. We have used the *Fewbody* numerical toolkit to perform the scattering interactions (Fregeau et al. 2004). For calculating the cross sections, we use a generalization of the technique described in McMillan & Hut (1996) in which for each annulus in impact parameter we perform only one scattering interaction, instead of the many required by their technique. This allows us to more precisely calculate the uncertainties in the cross sections, in particular yielding accurate asymmetric error bars. To handle the small number statistics, we use the tables in Gehrels (1986).

Figure 3 shows the dimensionless cross sections,  $\sigma/\pi a^2$ , for the outcomes involving no collisions in Table 1, as a function of  $v_\infty/v_c$  for a planetary system with mass ratio  $q = 10^{-3}$  and  $e = 0$ , and with  $M_1 = M_2 = M$ . Points plotted are as described in the legend. Circles represent resonant interactions, while triangles represent non-resonances (“direct” interactions). The error bars plotted are one-sigma. The vertical dotted lines are the critical velocity and orbital speed. The solid lines are the analytically predicted cross sections from section 2, while the dashed line is the order of magnitude estimated cross section from the same section. We have calculated the same cross sections using *Starlab* (McMillan & Hut 1996; Portegies Zwart et al. 2001), and the agreement is excellent. Note that with the exception of section 6, all calculations presented in this paper are performed with  $e = 0$ . Previous results show that most cross sections of interest do not depend strongly on eccentricity (Hut & Bahcall 1983). Indeed, we have calculated the cross sections in Figure 3 using a thermal eccentricity distribution and

find only a slight increase in the resonant cross sections (and corresponding decrease in the non-resonant cross sections) relative to the  $e = 0$  case.

Looking first at the region  $v_\infty > v_{\text{orb}}$ , we see  $\sigma_{\text{ion}}$  plotted in blue and  $\sigma_{\text{ex},s(\text{non-res})}$  plotted in red, along with the corresponding analytically predicted cross sections (eqs. [13] and [14], respectively) plotted as solid lines. The agreement is clearly quite excellent.

Next, looking at the region  $v_\infty < v_c$ , we see  $\sigma_{\text{ex-p}(\text{res})}$  (circles) and  $\sigma_{\text{ex-p}(\text{non-res})}$  (triangles) plotted in green, with the corresponding analytically predicted result of eq. (6) (the two cross sections are expected to be roughly equal, from eq. [5]) plotted as a solid line.  $\sigma_{\text{ex-p}(\text{res})}$  and  $\sigma_{\text{ex-p}(\text{non-res})}$  appear to be roughly equal, with  $\sigma_{\text{ex-p}(\text{res})}$  larger by  $\sim 10\%$  for  $v_\infty \ll v_c$ , while the analytical prediction is roughly  $\sim 50\%$  larger than the numerical result. Plotted in red triangles is  $\sigma_{\text{ex},s(\text{non-res})}$ , along with the corresponding analytical result from eq. (7) plotted as a solid line. Clearly the agreement is superb. Plotted in red circles is the resonant cross section  $\sigma_{\text{ex},s(\text{res})}$ , with the analytical result from eq. (10) plotted as a solid line. Although the statistics on this very small cross section are not as good as the other cross sections for  $v_\infty < v_c$ , it still appears to agree very well with the analytical prediction. Finally, plotted in black circles is  $\sigma_{\text{pres}(\text{res})}$ . Although from eq. (11) above we expect it to be equal to  $\sigma_{\text{ex},s(\text{res})}$ , it is larger by nearly an order of magnitude. The discrepancy is due to the operational definition of resonance we have used—namely that the mean-squared separation of all bodies makes more than one minimum, with a successive minimum counted only if the intervening maximum between it and the previous minimum is at least twice the value of both minima (McMillan & Hut 1996). Clearly this definition is too liberal, and classifies some preservation outcomes as resonant when they should not be classified as such. In fact, requiring that the mean-squared separation make more than two minima for a resonance decreases  $\sigma_{\text{pres}(\text{res})}$  by about an order of magnitude, bringing it into agreement with the analytical prediction and making it nearly equal to  $\sigma_{\text{ex},s(\text{res})}$ . Requiring that intervening maxima be four times (instead of twice) the value of the minima on either side for a successive minimum to be counted has no discernible effect on the results.

In the region  $v_c < v_\infty < v_{\text{orb}}$  resonance is, of course, forbidden. The cross section  $\sigma_{\text{ex-p}(\text{non-res})}$  drops off quickly above  $v_\infty = v_c$ , obeying roughly

$$\frac{\sigma_{\text{ex-p}(\text{non-res})}}{\pi a^2} \approx 1.5 \times 10^3 \left( \frac{v_\infty}{v_c} \right)^{-6}, \quad (16)$$

for the case  $M_1 = M_2 = M$ , and  $q = m/M = 10^{-3}$ . The cross sections for ionization and exchange of the incoming star for the host star (plotted in blue and red, respectively) are of the same order of magnitude, and only slightly different from the order of magnitude estimate in eq. (15) (shown in the dashed line). In particular, for the bulk of the region,  $\sigma_{\text{ion}} \approx 2\sigma_{\text{ex},s(\text{non-res})}$ , and  $\sigma_{\text{ion}}$  is  $\sim 20\%$  larger than the order of magnitude estimate, yielding

$$\sigma_{\text{ion}} \approx 1.2\pi a \frac{GM_t}{v_\infty^2}, \quad (17)$$

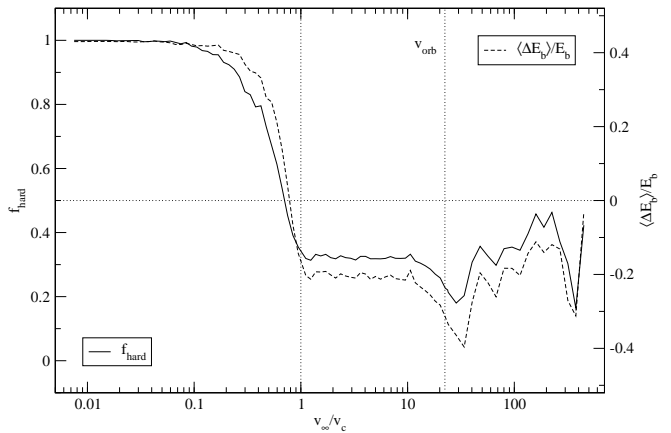


FIG. 4.— Statistics on the final planetary systems formed via non-resonant exchange in which the planet’s original host star is ejected (“ex\_s (non-res)”), as a function of  $v_\infty/v_c$ , for the case  $M_1 = M_2 = M$  and  $q = 10^{-3}$ . The fraction of final planetary systems that have hardened (semimajor axis decreased),  $f_{\text{hard}}$ , is shown in the solid line. The average change in the binding energy of the planetary system,  $\langle \Delta E_b \rangle / E_b = \langle GMm/2a' - GMm/2a \rangle / (GMm/2a) = a(1/a') - 1$ , is shown in the dashed line. The vertical dotted lines are the critical velocity and the orbital speed. The horizontal dotted line represents the value 0.5 for  $f_{\text{hard}}$  and 0 for  $\langle \Delta E_b \rangle / E_b$ . The hard-soft boundary lies where  $f_{\text{hard}}$  crosses 0.5, and  $\langle \Delta E_b \rangle / E_b$  crosses 0, which clearly and robustly occurs at  $v_\infty \approx 0.75v_c$ .

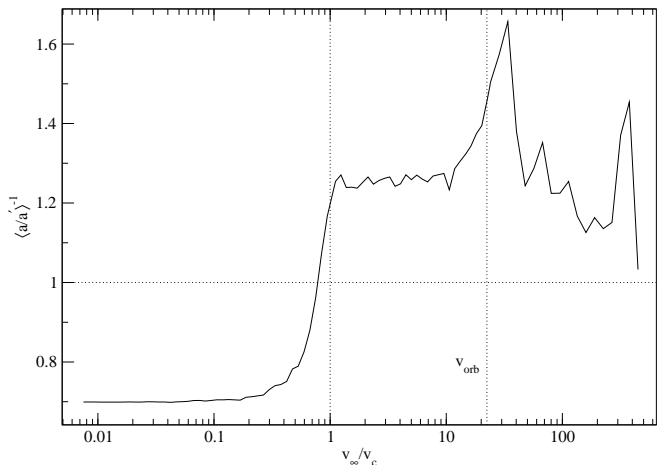


FIG. 5.— The quantity  $\langle a/a' \rangle^{-1}$ , the inversely-weighted average of the ratio of the planetary system’s final semimajor axis  $a'$  to its initial value  $a$ , as a function of  $v_\infty/v_c$  for the planetary systems formed via non-resonant exchange in which the planet’s original host star is ejected (“ex\_s (non-res)”), for the case  $M_1 = M_2 = M$  and  $q = 10^{-3}$ . The vertical dotted lines show  $v_c$  and  $v_{\text{orb}}$ , while the horizontal dotted line shows the value 1.

and

$$\sigma_{\text{ex},s(\text{non-res})} \approx 0.6\pi a \frac{GM_t}{v_\infty^2}, \quad (18)$$

again, for the case  $M_1 = M_2 = M$ , and  $q = m/M = 10^{-3}$ . However, as discussed above in section 2, we expect the test-particle limit to be reached at  $q \approx 10^{-1}$ , so the results here should be valid for all  $q \lesssim 10^{-1}$ .

#### 4. PROPERTIES OF EXCHANGE SYSTEMS AND THE HARD-SOFT BOUNDARY

Having determined the character of the scattering interactions in each region of parameter space shown in

Fig. 1, we now consider the properties of the final planetary system for the outcomes which yield a planetary system—namely resonant preservation, and exchange of the host star for the incoming star. Since resonance is only allowed for  $v_\infty < v_c$ , for simplicity we consider only the outcome “ex<sub>s</sub> (non-res)”, which has a significant cross section for all  $v_\infty$ . Shown in Figure 4 are the statistical properties of the final planetary systems in the outcome “ex<sub>s</sub> (non-res)” as a function of  $v_\infty/v_c$ , for the case  $M_1 = M_2 = M$ ,  $q = 10^{-3}$  and  $e = 0$ . The fraction of final planetary systems that have hardened (semimajor axis decreased),  $f_{\text{hard}}$ , is shown in the solid line. The average change in the binding energy of the planetary system,  $\langle \Delta E_b \rangle / E_b = \langle GMm/2a' - GMm/2a \rangle / (GMm/2a) = a \langle 1/a' \rangle - 1$ , is shown in the dashed line. The vertical dotted lines are the critical velocity and the orbital speed. The horizontal dotted line represents the value 0.5 for  $f_{\text{hard}}$  and 0 for  $\langle \Delta E_b \rangle / E_b$ . For  $v_\infty \ll v_c$ , every outcome results in the planetary system hardening, with  $\langle \Delta E_b \rangle / E_b \approx 0.4$ . This implies that the semimajor axis has shrunk to about 70% of its initial value, as shown in Figure 5, which plots  $\langle a/a' \rangle^{-1}$  as a function of  $v_\infty/v_c$ . In the region  $v_c < v_\infty < v_{\text{orb}}$ , the planetary system predominantly widens as a result of the encounter, with only  $\approx 30\%$  of systems hardening. The systems don’t widen by much, on average decreasing their energy by about 20%. This corresponds to an increase in the semimajor axis of about 25%, as shown in Figure 5. This is rather interesting, since in this region exchange is nearly as likely as ionization, implying that a significant fraction of systems that undergo a strong dynamical encounter survive it. And those that survive suffer a comparatively small change in their semimajor axis, with a significant fraction actually hardening. Finally, in the region  $v_\infty > v_{\text{orb}}$ , since the cross section for ionization is several orders of magnitude larger than that of exchange, the statistics are too poor to say anything conclusive. Although the curves in Figures 4 and 5 appear to begin to rebound, we expect that they actually go smoothly to  $f_{\text{hard}} = 0$ ,  $\langle \Delta E_b \rangle / E_b = -1$ , and  $\langle a/a' \rangle^{-1} \rightarrow \infty$ .

As described in section 2, there has been considerable variance in the literature on what velocity demarcates the hard–soft boundary for systems with a wide mass ratio. A look at Figure 4 reveals that (at least for  $M_1 = M_2$ ), the hard–soft boundary—which lies where  $f_{\text{hard}}$  crosses 0.5 and  $\langle \Delta E_b \rangle / E_b$  crosses 0—robustly occurs at  $v_\infty \approx 0.75v_c$ . Of course, simply stating that the hard–soft boundary lies at  $v_\infty \approx 0.75v_c$  belies the fact that for  $v_c < v_\infty < v_{\text{orb}}$  the likelihood of a planetary system surviving a strong dynamical encounter in some form is rather significant.

Based on the understanding garnered from our analysis thus far, it is useful to consider the fate of a planetary system subject to strong dynamical encounters in a stellar environment of number density  $n$  and velocity dispersion  $v_\sigma$ . The average relative velocity between objects in such a system is roughly  $\sqrt{2}v_\sigma$ , but since we are interested only in orders of magnitude here we will take  $v_\infty = v_\sigma$ . Since we know all relevant cross sections, we can perform a simple “ $n\sigma v$ ” estimate for the lifetime of a planetary system as a function of  $a$ ,

$$\tau = \frac{1}{n\sigma v_\infty}, \quad (19)$$

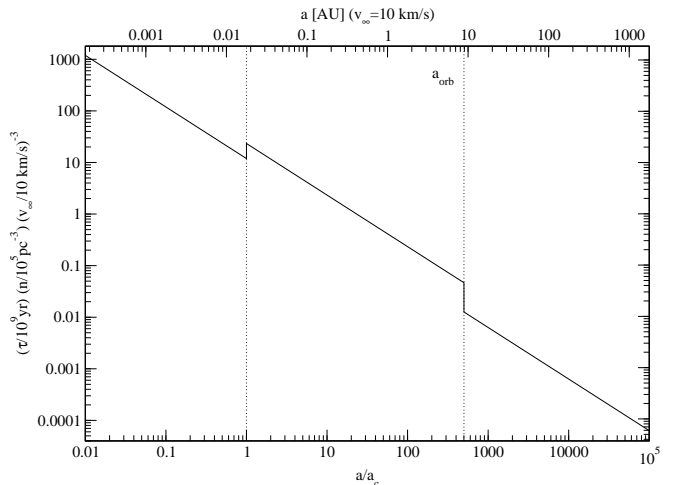


FIG. 6.— The characteristic lifetime  $\tau$ , plotted in the quantity  $\tau n / v_\infty^3$  (see eq. [22]), of a planetary system with mass ratio  $q = 10^{-3}$ , host star mass  $M = M_\odot$ , and eccentricity  $e = 0$  in a stellar environment of number density  $n$  and velocity dispersion  $v_\infty$ , as a function of  $a/a_c$ . The critical semimajor axis  $a_c$  is as defined in section 4 after eq. (22). The two vertical dotted lines show  $a = a_c$  and  $a = a_{\text{orb}}$ . The quantity  $a_{\text{orb}}$  is the value of  $a$  for which the orbital speed in the planetary system is equal to  $v_\infty$ .

which we do now. A useful way to think about the evolution of a planetary system subject to encounters is the following. Taking the masses to be given, for a given value of  $a$ , we know  $v_c$  and  $v_{\text{orb}}$  from eqs. (1) and (2). Given the value of  $v_\infty$  fixed by the velocity dispersion of the stellar environment in which the planetary system finds itself, we thus have  $v_\infty/v_c$  and know in which section of parameter space the planetary system lies in Figure 3. In the region  $v_\infty < v_c$ , by far the most likely outcome of a strong dynamical interaction is exchange in which the planet is ejected. Thus  $\tau$  for this region can be calculated using the cross section  $\sigma_{\text{ex-p}} = \sigma_{\text{ex-p(res)}} + \sigma_{\text{ex-p(non-res)}}$ . In the region  $v_\infty > v_{\text{orb}}$  the dominant outcome is ionization, so one uses  $\sigma_{\text{ion}}$  in eq. (19). In between, in  $v_c < v_\infty < v_{\text{orb}}$ , the outcomes “ion” and “ex<sub>s</sub> (non-res)” are almost equally likely. From eqs. (17) and (18), roughly  $X_i \equiv 2/3$  of strong dynamical interactions result in ionization, while the remaining  $X_e \equiv 1/3$  result in non-resonant exchange of the host star for the incoming star. The systems that undergo exchange suffer only a small perturbation to their orbital size, as evidenced by Figure 5. As  $a$  changes,  $v_c$  and  $v_{\text{orb}}$  scale as  $a^{-1/2}$  with  $v_c/v_{\text{orb}}$  fixed. Thus, in effect, as  $a$  changes, the quantity  $v_\infty/v_c$  scales as  $a^{1/2}$  with the distance between  $v_c$  and  $v_{\text{orb}}$  held fixed in log-space, and so the planetary system simply occupies a new position on the  $x$ -axis in Figure 3. A planetary system lying in regions  $v_\infty < v_c$  or  $v_\infty > v_{\text{orb}}$  is destroyed as a result of an interaction. But for a planetary system in the intermediate region, it is destroyed a fraction  $X_i$  of the time, while the other fraction  $X_e$  of the time it survives with  $v_\infty/v_c$  increased by a mere  $\sim 10\%$  on average (from Figure 5). Eventually systems that survive via many exchange interactions will find themselves in the region  $v_\infty > v_{\text{orb}}$  and be destroyed quickly by ionization. Since the average change in  $a$  due to these exchanges is rather

small, let us, for the sake of simplifying the calculation of  $\tau$ , assume that they survive indefinitely. The average lifetime in this region of parameter space, including both ionization and exchange, is thus

$$\tau = \tau_i + X_e \tau_i + X_e^2 \tau_i + X_e^3 \tau_i + \dots = \frac{\tau_i}{1 - X_e}, \quad (20)$$

where

$$\tau_i = \frac{1}{n(\sigma_{\text{ion}} + \sigma_{\text{ex, s(non-res)}})v_\infty}. \quad (21)$$

Since all cross sections of interest here scale as  $\sigma = \sigma_0 a/v_\infty^2$  where  $\sigma_0$  is a function of the masses, we can be quite general and plot

$$\frac{\tau n}{v_\infty^3} = \frac{1}{\sigma_0} \left( \frac{a}{a_c} \right)^{-1} \frac{\mu}{GM_1 m}, \quad (22)$$

where the critical semimajor axis is  $a_c = GM_1 m/\mu v_\infty^2$ , as a function of  $a/a_c$  in Figure 6. Note that the sharpness of the transitions at  $a = a_c$  and  $a = a_{\text{orb}}$  is due to the use of the analytical cross sections in calculating the lifetimes. From the numerical cross sections in Figure 3 it is evident that, in reality, the transitions are a bit smoother, although the general structure is the same. Clearly the overall trend is for the lifetime to scale as  $a^{-1}$ , with the coefficient varying by only a factor of a few among the different regions of parameter space. Using only the fact that the hard–soft boundary lies at  $v_\infty = v_c$ , one might expect the lifetime to drop markedly at  $a = a_c$ . In fact, it increases slightly there, and does not drop until  $a = a_{\text{orb}}$ , due to the large cross section for planetary system preserving exchange in the intermediate regime. We now consider the implications of this result.

## 5. IMPLICATIONS

The main implication of our results is that the minimum size of planetary systems that will likely be destroyed as a result of dynamical interactions in dense stellar environments is larger than has previously been assumed. This limit can be read almost directly from Figure 6 for a given velocity dispersion, stellar density, and timescale. For example, in a globular cluster like 47 Tuc, which has a central stellar density of  $\sim 10^5 \text{ pc}^{-3}$  and velocity dispersion of  $\sim 10 \text{ km/s}$ , planetary systems wider than 0.05 AU will have been destroyed after  $\sim 10 \text{ Gyr}$ . The second implication is that the statement that the location of the hard–soft boundary is at  $v_\infty = v_c$ , although correct, when taken on its own can be misleading. It is true that planetary systems on the low-velocity side of the hard–soft boundary that survive interactions tend to harden on average. However, planetary systems are overwhelmingly likely to be destroyed in this regime, as can be read directly from the cross sections in Figure 3. Similarly, although planetary systems tend to soften, on average, for  $v_\infty > v_c$ , it is not until  $v_\infty > v_{\text{orb}}$  that ionization dominates the outcome. In other words, there is a wide region in parameter space (from  $v_\infty = v_c$  to  $v_\infty = v_{\text{orb}}$ ) for which the probability of exchange in which a planetary system results is comparable that of ionization, and those resulting planetary systems soften by only a small amount (as shown in Figures 4 and 5).

Our results have a bearing on previous studies in the literature in which authors have adopted inappropriate prescriptions for outcomes of scattering interactions with

planetary systems. As an example, Bonnell et al. (2001) calculated the evolution of a population of planetary systems in stellar environments of differing density, using a Monte-Carlo approach in which planetary systems undergo binary–single interactions with field stars. As a result of each interaction, the planetary system is assumed to be ionized if  $v_\infty > v_c$ , and to harden if  $v_\infty < v_c$ . However, as our results show, for  $v_\infty < v_c$  those planetary systems undergoing strong interactions are destroyed, for  $v_c < v_\infty < v_{\text{orb}}$  they have an increased probability of surviving, and for  $v_\infty > v_{\text{orb}}$  they are predominantly ionized. The result of the discrepancy is that most of the systems destroyed on the high-velocity side of the hard–soft boundary ( $v_\infty = v_c$ ) in these simulations will actually survive as planetary systems of some kind. The growth of a spike in the relative frequency of planetary systems smaller than  $a_c$  predicted in low velocity dispersion systems (such as open clusters), should not occur, with the distribution of semimajor axes dropping smoothly from  $a_c$  to  $a_{\text{orb}}$ . There is the possibility for a slight hump in the relative frequency of planets with  $a_c < a < a_{\text{orb}}$ , based on our Figure 6, but it would not be nearly as pronounced as what is shown in Figure 5 of Bonnell et al. (2001).

On the observational side, we find that of the hot Jupiter planetary systems expected to be detected in 47 Tuc in the transit survey of Gilliland et al. (2000)—which was sensitive to periods up to  $\approx 4 \text{ d}$ —essentially all are expected to survive dynamical interactions in the high density core of the cluster on timescales comparable to the age of the cluster. This can be read directly from Figure 6 with  $a \approx 0.05 \text{ AU}$ . This bolsters the conclusion drawn by Weldrake et al. (2005) that it is not dynamics that is responsible for the lack of hot Jupiters detected in 47 Tuc, but rather may be metallicity-dependent effects (Fischer & Valenti 2005). The Weldrake et al. study sampled regions outside the core and was sensitive to orbital periods up to  $\approx 16 \text{ d}$ , so the hot Jupiter binaries they looked for would also not have been destroyed by dynamical interactions due to the lower density there. However, it is possible that they would have been destroyed early in the lifetime of the cluster if it went through a high-density phase early on, the possibility of which is discussed in Bonnell et al. (2001).

Looking ahead, we now speculate on future possibilities for observations of planets in dense stellar environments. The globular cluster Terzan 5 is unique in that it has super-solar metallicity. Any argument against the formation of planets in globular clusters due to metallicity effects is null in Terzan 5. If we adopt the frequency of hot Jupiters in the solar neighborhood of 0.8% (Butler et al. 2000; Basri 2004), and use the estimated central number density of  $10^5 \text{ pc}^{-3}$  and core radius of 0.5 pc (Harris 1996), we expect  $\sim 100$  hot Jupiters in orbit around main sequence stars in the core of Terzan 5. According to Figure 6 for  $v_\infty = 10 \text{ km/s}$ , all of these systems would survive for a Hubble time, since the definition of “hot Jupiter” implies an orbit period less than  $\sim 10 \text{ d}$ . Terzan 5 lies nearly in the Galactic disk, close to the Galactic center, making optical observations of it practically impossible. However, it is readily observed in radio wavelengths, and already many millisecond pulsars (MSPs) have been discovered in it (Ransom et al. 2005). There is thus the possibility of detecting planets

in orbits around MSPs in this cluster. The most natural formation mechanism involves exchanging the MSP for the planet’s host star in a dynamical interaction. From Figure 1 we see that for the velocity dispersion of Terzan 5 planetary systems with  $a \sim 0.01\text{--}10\text{ AU}$  lie in the intermediate regime, and are thus most likely to possibly have exchanged in a MSP. The formation of such systems is a balancing act between destruction (for the wider systems) and a long interaction timescale (for the smaller systems), with a “sweet spot” at  $a \sim 0.1\text{ AU}$ . Although the expected number of MSP-planet systems is small (probably  $\sim 1$ ), we can predict that such a system would have  $a \sim 0.1\text{ AU}$ . There is also the possibility that planets could form around pulsars, but the frequency of formation is rather less certain (Sigurdsson 1992).

## 6. PSR B1620-26

The planetary system PSR B1620-26 in the globular cluster M4 consists of a Jovian-mass object in an  $\approx 20\text{ AU}$  orbit about a MSP–WD binary. The planetary system sits right at the edge of the core of M4 in projection, which has a central velocity dispersion of  $\approx 4\text{ km/s}$ . Looking at Figure 1, we see that the planetary system lies comfortably in the “intermediate” regime, making it very likely that it was formed via a dynamical scattering interaction in which the NS-containing binary exchanged into the planetary system (as one unit) in place of the planet’s original host star (scenario “2” below). With this motivation, we now perform a detailed numerical analysis of the possible formation scenarios of PSR B1620-26.

First, it is useful to list the physical parameters of the system. The pulsar has a spin period of  $\approx 11\text{ ms}$  and mass  $\approx 1.35 M_\odot$ , while the WD has mass  $0.34 \pm 0.04 M_\odot$ . Hubble Space Telescope data has confirmed that the WD is young, with an age of  $\sim 0.5\text{ Gyr}$ . The PSR–WD binary has eccentricity  $\sim 0.025$ . The planet has mass  $\approx 1\text{--}3M_J$ , where  $M_J$  is the mass of Jupiter, and orbits with eccentricity  $\sim 0.3$  about the MSP–WD binary. The inclination between the inner and outer orbits is  $\sim 55^{+14}_{-8}$ . The currently favored dynamical formation scenarios are the following. In what we will call scenario “1”, a binary composed of a WD and a NS undergoes an exchange interaction with a binary consisting a main-sequence star near the turn-off mass and a Jovian planet. In the encounter the WD is ejected from the system with the normal star exchanging into orbit with PSR, leaving the planet in a wide orbit about the star–PSR binary. The star then undergoes mass transfer as it goes through the red giant phase, recycling the PSR to millisecond periods (Sigurdsson et al. 2003). In scenario “2”, a binary composed of a NS and a near turn-off main-sequence star of mass  $0.8 M_\odot$  undergoes an exchange interaction with a binary composed of a main-sequence star and a Jovian planet. In the encounter the NS–star binary acts as a single unit and exchanges into the planet orbit, ejecting the planet’s original host star. The star then undergoes mass transfer as it goes through the red giant phase, recycling the PSR to millisecond periods (Ford et al. 2000). As we discuss below, our expectation that scenario “2” is the much more likely one proves to be correct.

### 6.1. Quantifying the Outcome Likelihoods

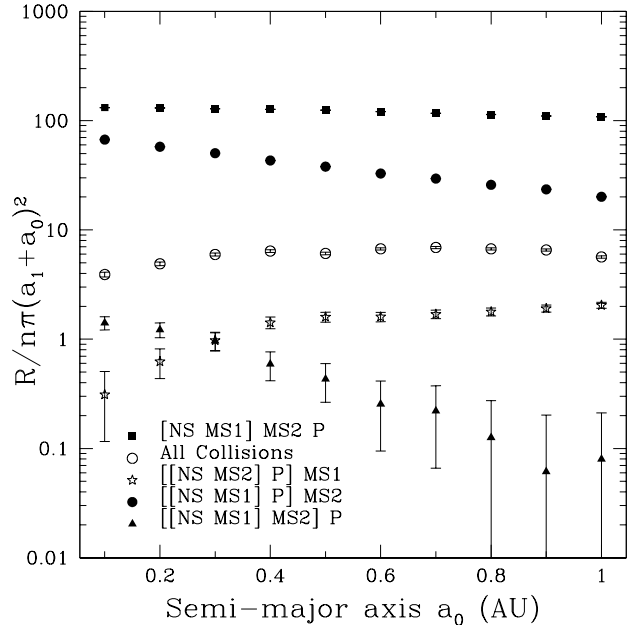


FIG. 7.— Quantifying the likelihood of the possible formation scenarios of PSR B1620-26: The semi-normalized rate  $R/[n\pi(a_0 + a_1)^2]$  (in units of  $\text{km/s}$ ) for various outcomes of a scattering interaction between a NS–MS1 binary and a MS2–P planetary system as a function of  $a_0$ , the semi-major axis of the NS–MS1 binary. Points are as defined in the legend. The rate for scenario “2” (“[[NS MS1] P] MS2”) clearly dominates over scenario “1” (“[[NS MS2] P] MS1”) for a wide range in  $a_0$ .

As in section 3, we use the *Fewbody* numerical toolkit to perform scattering interactions and calculate cross sections for different outcomes. The interaction rate per planetary system is simply

$$R = \int_0^\infty dv_\infty f(v_\infty) n \sigma v_\infty, \quad (23)$$

where  $f(v_\infty)$  is the velocity distribution function,  $n$  is the number density of NS binaries, and  $\sigma$  is the cross section for the outcome of interest. Rates presented below were calculated by discretizing the integral over the distribution function and summing over a range of velocities wide enough to guarantee convergence. In particular, we typically integrate over a range of velocities from  $1\text{ km/s}$  to  $15\text{ km/s}$ , with the upper limit set by the escape speed of  $15.25\text{ km/s}$  of the cluster (Beer et al. 2004). For the distribution function we assume a simple Maxwellian with a velocity dispersion of  $v_\infty = \sqrt{2}v_\sigma$ , where  $v_\sigma = 3.88\text{ km/s}$  is the velocity dispersion in the core of M4 and the factor of  $\sqrt{2}$  is due to the fact that we are considering relative velocities between pairs of objects. Our naming convention for the objects is analogous to what we used above, with “[NS MS1] [MS2 P]” denoting the initial configuration of the two binaries before the scattering interaction. “MS1” in fact represents a WD in scenario “1” and a main-sequence star in scenario “2”; however, we label it “MS1” in both cases since it is only the mass of the object that matters in the scattering interactions (the radius of the object plays only a minor role when direct physical collisions are considered). We label the semi-major axis of the NS–MS1 binary  $a_0$ , and that of the

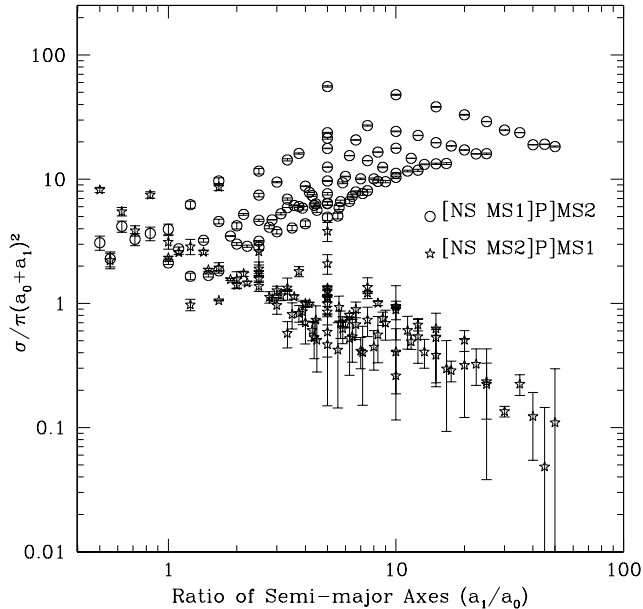


FIG. 8.— The normalized cross section,  $\sigma/\pi(a_0+a_1)^2$ , for PSR B1620-26 formation scenarios “1” (stars) and “2” (circles) as a function of  $a_1/a_0$ , where  $a_0$  is the initial semimajor axis of the neutron star binary and  $a_1$  is that of the planet binary. The cross sections are calculated over a large grid in  $a_0$ - $a_1$  space, hence their multi-valued nature as a function of  $a_1/a_0$ . All interactions were performed with  $v_\infty = 5$  km/s since the velocity-dependent rate peaks at this value. It is clear from the figure that as long as  $a_1 \gtrsim a_0$ , which is quite reasonable on physical grounds, scenario “2” is the most likely.

MS2-P binary  $a_1$ . Since the NS binary must be significantly tighter than the planet binary, it is expected to behave dynamically as a single unit; thus the cross sections for different outcomes are expected to scale with  $a_1$  (our numerical results confirm this). We therefore vary only  $a_0$ , from 0.1 AU to 1 AU (a typical range of values), and keep  $a_1$  fixed at 5 AU. We fix  $e_1$ , the eccentricity of the planet binary, at 0, while we draw  $e_0$ , the eccentricity of the NS binary from a thermal distribution truncated at large  $e_0$  such that neither object in the binary exceeds its Roche lobe. Figure 7 shows the semi-normalized rate  $R/[n\pi(a_0+a_1)^2]$  (in units of km/s) for the different outcomes listed in the legend as a function of  $a_0$ . The most likely outcome is “[NS MS1] MS2 P”, i.e., destruction of the planetary system with preservation of the NS binary. The next most likely outcome is scenario “2” (“[[NS MS1] P] MS2”), confirming our expectations from above. The next is any outcome involving direct physical collisions between system members, which we lump together into one category for the sake of succinctness. The next is scenario “1” (“[[NS MS2] P] MS1”) which is larger than “[NS MS1] MS2 P” only for  $a_0 \gtrsim 0.3$  AU.

To verify that our results are not dependent on the choice of  $a_1$ , we now consider the relative probabilities for scenarios “1” and “2” over a large grid in  $a_0$ - $a_1$  space. To simplify the presentation of the results we plot the normalized cross section for each outcome,  $\sigma/\pi(a_0+a_1)^2$ , as a function of  $a_1/a_0$ , as shown in Figure 8, hence the multi-valued nature of the cross sections. For simplicity

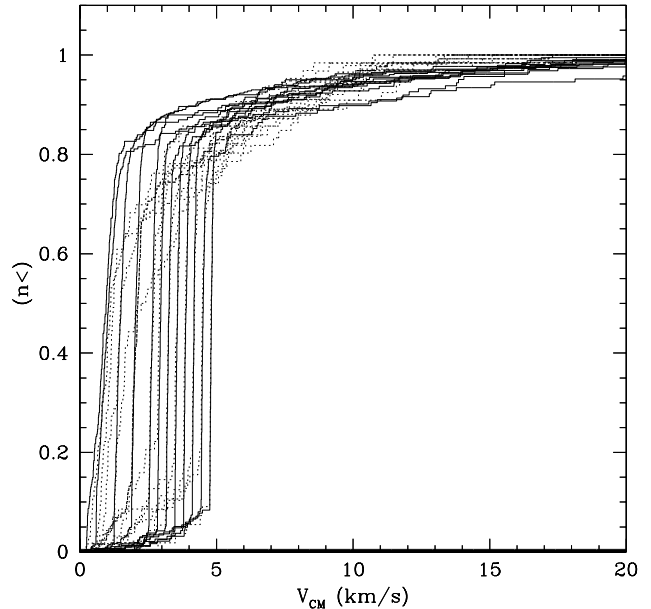


FIG. 9.— The cumulative distribution of the center-of-mass velocity of the putative PSR B1620-26 triple after the exchange interaction in scenario “2”, for the cases  $a_0 = 0.1$  AU (solid lines) and  $a_0 = 1$  AU (dotted lines) for several values of  $v_\infty$  from 1 km/s (left-most) to 15 km/s (right-most). In both cases we set  $a_1 = 5$  AU. The triple system appears to suffer a recoil of  $\sim 3$  km/s, which is clearly not enough to eject it from the cluster (requiring  $\approx 15$  km/s), but may be enough to displace it significantly away from the core.

all interactions were performed with  $v_\infty = 5$  km/s since the velocity-dependent rate peaks at this value. It is clear from the figure that as long as  $a_1 \gtrsim a_0$ , which is quite reasonable on physical grounds, scenario “2” is the most probable. For the physically most reasonable value of  $a_1/a_0 \approx 10$ , scenario “2” is more probable by more than an order of magnitude over scenario “1”.

Having confirmed the preferred formation scenario, we now consider the orbital parameters of the hierarchical triple formed. Figure 9 shows the cumulative distribution of the center-of-mass velocity of the triple after the exchange interaction, for the cases  $a_0 = 0.1$  AU (solid lines) and  $a_0 = 1$  AU (dotted lines) for several values of  $v_\infty$  from 1 km/s (left-most) to 15 km/s (right-most). The triple system appears to suffer a recoil of  $\sim 3$  km/s, which is clearly not enough to eject it from the cluster (requiring  $\approx 15$  km/s), but may be enough to eject it from the core. Figures 10 and 11 show the cumulative distributions of outer semimajor axis,  $a_{\text{out}}$ , and eccentricity,  $e_{\text{out}}$ , respectively, with the same convention for the line types as in the previous figure. The outer semimajor axis is clearly not particularly dependent on either  $a_0$  or  $v_\infty$ , with a peak at  $\sim 10$  AU. The outer eccentricity, on the other hand, while not particularly dependent on  $v_\infty$ , is strongly dependent on  $a_0$ . For  $a_0 = 0.1$  AU the eccentricity distribution is roughly thermal, with the cumulative distribution  $\propto e_{\text{out}}^2$ . For  $a_0 = 1$  AU the eccentricity distribution is flatter, with more systems at lower eccentricity. This result suggests that of the two,  $a_0 = 1$  AU is the favored value for the NS binary semimajor axis, since

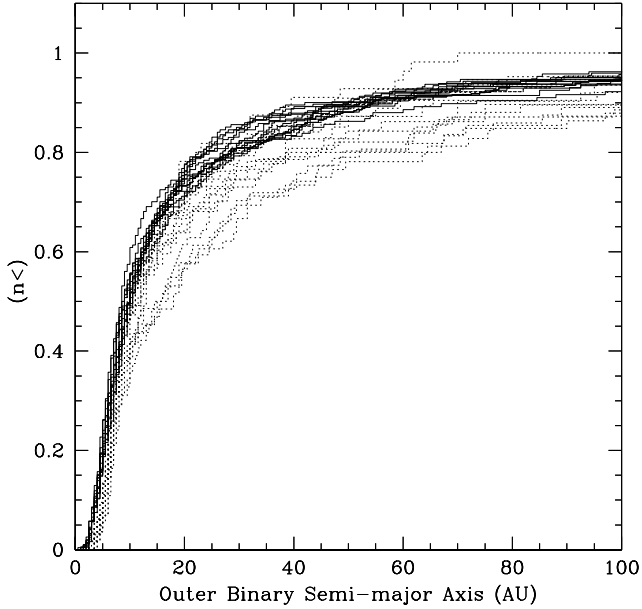


FIG. 10.— The cumulative distribution of the outer semimajor axis,  $a_{\text{out}}$ , for the putative PSR B1620-26 triple system formed in scenario “2”. Line conventions and initial conditions are the same as in Figure 9.

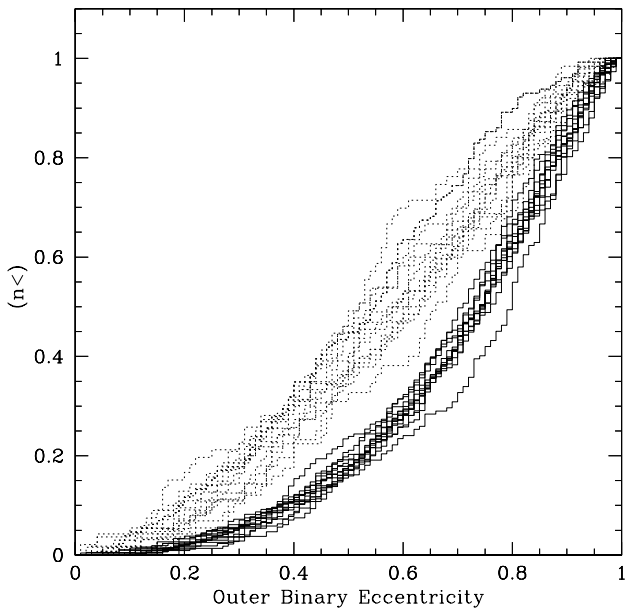


FIG. 11.— The cumulative distribution of the outer eccentricity,  $e_{\text{out}}$ , for the putative PSR B1620-26 triple system formed in scenario “2”. Line conventions and initial conditions are the same as in Figure 9.

we know from observations that the outer eccentricity is rather low, with  $e_{\text{out}} \sim 0.2 \pm 0.1$  (Sigurdsson & Thorsett 2004). In Figure 12 we show the cumulative distribution of the inner binary semimajor axis,  $a_{\text{in}}$ , with the same convention for the line types as in the previous figures. Confirming our earlier assumption, the inner bi-

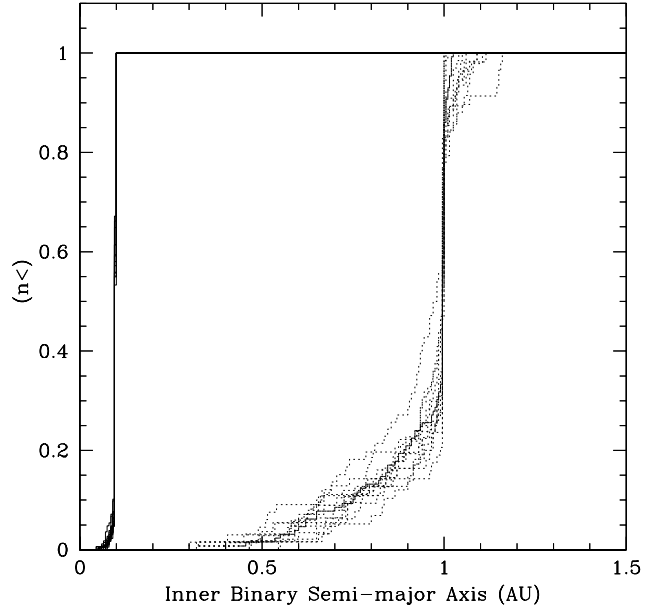


FIG. 12.— The cumulative distribution of the inner semi-major axis,  $a_{\text{in}}$ , for the putative PSR B1620-26 triple system formed in scenario “2”. Line conventions and initial conditions are the same as in Figure 9.

nary clearly behaves as a single dynamical unit, with the distributions for the final values strongly peaked around their initial values, and with very minimal dependence on  $v_{\infty}$ .

## 6.2. Evolution of the Hierarchical Triple Due to Mass Transfer

In scenario “2”, the hierarchical triple formed via the dynamical interaction is not the planetary system we see today in M4, but merely its progenitor. In this section we calculate the effects on the triple due to mass transfer in the inner binary as the main-sequence star ascends the red giant branch, and apply the results to the ensemble of triples formed in our scattering interactions. We assume slow isotropic mass loss, and that during this process the eccentricities remain invariant (Rasio et al. 1992). For the sake of simplifying the calculation we also assume that the inner and outer eccentricities are zero. Since the outer orbit carries so little angular momentum ( $\sim 0.4\%$  of the total angular momentum of the triple system) we neglect angular momentum coupling between the two orbits and treat them as two separate binaries during the mass transfer.

The angular momentum of the inner orbit is given by

$$L_{\text{in}} = M_{\text{NS}} M_{\text{MS1}} \left( \frac{G a_{\text{in}}}{M_{\text{in}}} \right)^{1/2}, \quad (24)$$

where  $M_{\text{in}} = M_{\text{NS}} + M_{\text{MS1}}$ ,  $M_{\text{NS}}$  and  $M_{\text{MS1}}$  are the masses of the NS and the WD progenitor star, respectively, and  $a_{\text{in}}$  is the semimajor axis of the inner binary. Similarly, the angular momentum of the outer orbit is given by

$$L_{\text{out}} = M_{\text{in}} M_{\text{P}} \left( \frac{G a_{\text{out}}}{M_{\text{T}}} \right)^{1/2}, \quad (25)$$

where  $M_T = M_{\text{in}} + M_P$ ,  $M_P$  is the mass of the planet, and  $a_{\text{out}}$  is the semimajor axis of the outer orbit. Taking the logarithm of both sides and differentiating, we get

$$\frac{\delta L_{\text{in}}}{L_{\text{in}}} = \frac{\delta M_{\text{NS}}}{M_{\text{NS}}} + \frac{\delta M_{\text{MS1}}}{M_{\text{MS1}}} + \frac{1}{2} \frac{\delta a_{\text{in}}}{a_{\text{in}}} - \frac{1}{2} \frac{\delta M_{\text{in}}}{M_{\text{in}}} \quad (26)$$

and

$$\frac{\delta L_{\text{out}}}{L_{\text{out}}} = \frac{\delta M_{\text{in}}}{M_{\text{in}}} + \frac{\delta M_P}{M_P} + \frac{1}{2} \frac{\delta a_{\text{out}}}{a_{\text{out}}} - \frac{1}{2} \frac{\delta M_T}{M_T} \quad (27)$$

for differential changes in the inner and outer orbits.

In the mass transfer process, we assume that the mass lost from MS1 gets channeled into an accretion disk around the NS, and any mass lost from the system is lost from the accretion disk with the characteristic angular momentum of the NS (see e.g. Podsiadlowski et al. 2002). This implies that

$$\delta L_{\text{in}} = a_{\text{in}}^2 \frac{M_{\text{MS1}}^2}{M_{\text{in}}^2} \Omega_{\text{in}} \delta M_{\text{in}}, \quad (28)$$

where  $\Omega_{\text{in}}$  is the orbital velocity of NS, given by

$$\Omega_{\text{in}} = \left( \frac{GM_{\text{in}}}{a_{\text{in}}^3} \right)^{1/2}. \quad (29)$$

Similarly, as mass is lost from the inner binary in the mass transfer process the angular momentum of the outer binary will change according to

$$\delta L_{\text{out}} = a_{\text{out}}^2 \frac{M_P^2}{M_T^2} \Omega_{\text{out}} \delta M_T, \quad (30)$$

where  $\Omega_{\text{out}}$  is the orbital angular velocity of the inner binary in the outer orbit, and is given by

$$\Omega_{\text{out}} = \left( \frac{GM_T}{a_{\text{out}}^3} \right)^{1/2}. \quad (31)$$

We parameterize the mass loss by defining  $\beta$  as the fraction of mass lost from MS1 that is accreted by the NS, so that  $\delta M_{\text{NS}} = -\beta \delta M_{\text{MS1}}$  and  $\delta M_{\text{in}} = (1 - \beta) \delta M_{\text{MS1}}$ . Note that with our conventions  $\delta M_{\text{MS1}} < 0$ . Combining equations (24) through (31), converting  $\delta$ 's to differentials and integrating, we find (Podsiadlowski et al. 2002):

$$\frac{a'_{\text{in}}}{a_{\text{in}}} = \left( \frac{M'_{\text{MS1}}}{M_{\text{MS1}}} \right)^{-2} \left( \frac{M'_{\text{NS}}}{M_{\text{NS}}} \right)^{-2/\beta} \left( \frac{M'_{\text{in}}}{M_{\text{in}}} \right)^{-1} \quad \text{for } 0 < \beta \leq 1, \quad (32)$$

$$\frac{a'_{\text{in}}}{a_{\text{in}}} = \left( \frac{M'_{\text{MS1}}}{M_{\text{MS1}}} \right)^{-2} \left( \frac{M'_{\text{in}}}{M_{\text{in}}} \right)^{-1} \times \exp \left[ 2 \left( \frac{M'_{\text{MS1}} - M_{\text{MS1}}}{M_{\text{NS}}} \right) \right] \quad \text{for } \beta = 0, \quad (33)$$

and

$$\frac{a'_{\text{out}}}{a_{\text{out}}} = \left( \frac{M'_T}{M_T} \right)^{-1} \quad \text{for all } \beta. \quad (34)$$

We can apply the expressions in eqs. (32) through (34) to the ensemble of triples formed via scenario ‘‘2’’ to determine their properties after mass transfer. Figure 13 shows the cumulative distribution of the inner binary semi-major axis after mass transfer. The solid

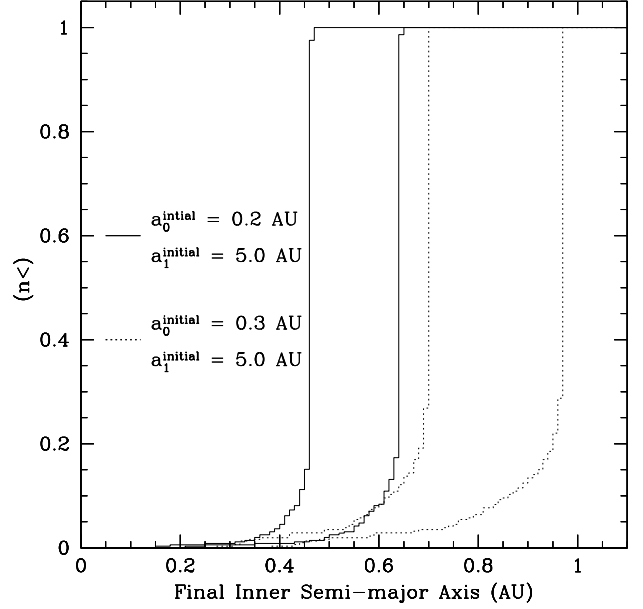


FIG. 13.— The cumulative distribution of the inner binary semi-major axis of the putative PSR B1620-26 triple system after mass transfer. The solid lines are for the case  $a_0 = 0.2$  AU—in other words, the NS–MS1 semimajor axis was 0.2 AU before the scattering interaction. The dotted lines are for the case  $a_0 = 0.3$  AU. In both cases we set  $a_1 = 5$  AU and  $v_\infty = 5$  km/s. For each set of the lines the rightmost represents completely non-conservative mass transfer ( $\beta = 0$ ), while the leftmost represents completely conservative mass transfer ( $\beta = 1$ ).

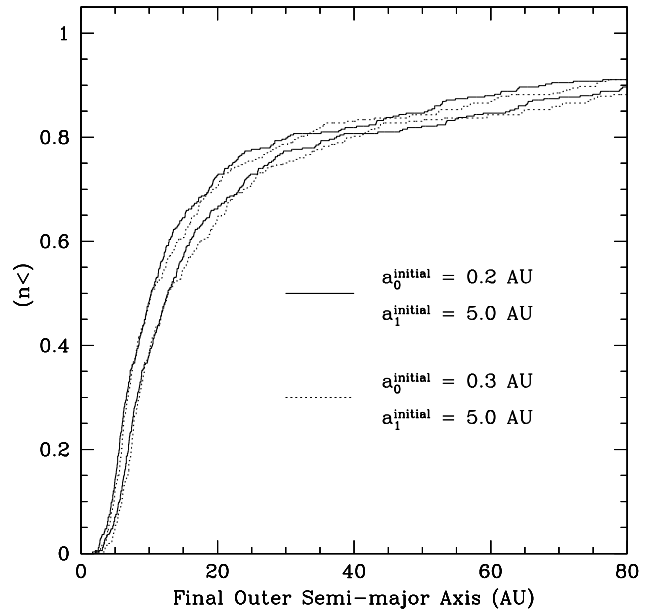


FIG. 14.— The cumulative distribution of the outer semi-major axis of the putative PSR B1620-26 triple system after mass transfer for the cases  $a_0 = 0.2$  AU (solid lines) and  $a_0 = 0.3$  AU (dotted lines). Line conventions and initial conditions are the same as in Figure 13.

lines are for  $a_0 = 0.2$  AU—in other words, the NS–MS1 semimajor axis was 0.2 AU before the scattering interaction. The dotted lines are for the case  $a_0 = 0.3$  AU. In both cases we set  $a_1 = 5$  AU and  $v_\infty = 5$  km/s. For each set of the lines the rightmost represents completely non-conservative mass transfer ( $\beta = 0$ ), while the leftmost represents completely conservative mass transfer ( $\beta = 1$ ). Figure 14 shows the cumulative distribution of the outer semi-major axis for the cases  $a_0 = 0.2$  AU and  $a_0 = 0.3$  AU. Line types are as in the previous figure. Comparing the distributions of the inner semimajor axis after the scattering interaction in Figure 12 with those after mass transfer in Figure 13, we see that the effect of mass transfer is to create a spread in the distribution of order the initial value. From observations we know the period of the inner orbit to be 191 d, corresponding to a semimajor axis of  $\approx 0.8$  AU (Sigurdsson & Thorsett 2004). From this figure we see that we can quite reasonably create such a system with  $a_0 \approx 0.3$  AU for a wide range in the mass transfer parameter  $\beta$ . From Figure 14 we see that the distribution of the outer semimajor axis after mass transfer is much broader. Although the peak in the distribution appears to occur around 5–10 AU, it is quite plausible to form a system with an outer semimajor axis of 20 AU, as we observe for the system today.

## 7. SUMMARY AND CONCLUSIONS

We have studied in detail dynamical scattering interactions between star–planet systems and other single stars, tabulating analytical cross sections for all possible outcomes of the scattering encounter, and confirming them with numerical experiments (as shown in Figure 3). In the scattering of planetary systems (or wide mass ratio binaries in general) there are two characteristic velocities in the problem (as shown in Figure 1): the critical velocity  $v_c$ , which is the value of  $v_\infty$  for which the total energy of the three-body system is zero; and  $v_{\text{orb}}$ , the orbital speed in the binary. For a mass ratio  $q \lesssim 10^{-3}$  the two characteristic velocities differ by more than an order of magnitude, opening up a region in parameter space in which the nature of the scattering process is fundamentally different from what occurs in comparable mass encounters. For  $v_c < v_\infty < v_{\text{orb}}$  two outcomes dominate the cross with roughly equal weight: ionization, which destroys the planetary system; and exchange of the incoming star for the planet’s original host star. Thus in this region—which does not exist for comparable mass systems—there is a significant probability that a planetary system undergoing a strong dynamical encounter survives, albeit with a new host star. Since in the past workers in the field have typically taken  $v_c$  as the velocity above which planetary systems are predominantly destroyed, this implies greater survivability of planetary systems in dense stellar environments than has been predicted in some cases, as the characteristic lifetime plotted in Figure 6 shows.

We have also numerically determined the location of the hard–soft boundary for planetary systems, and find that it lies at  $v_\infty \approx 0.75v_c$ . In other words, interactions with  $v_\infty < v_c$  in which the binary survives (e.g., via exchange) typically harden ( $a$  decreases), while for  $v_\infty > v_c$  surviving binaries soften ( $a$  increases). However, this simple statement belies the rich structure of the parameter space. In particular, for  $v_c < v_\infty < v_{\text{orb}}$ ,

although the surviving binary typically softens, it softens by only a small amount, increasing its semimajor axis by only  $\sim 25\%$ , as shown in Figure 5. Its final eccentricity, of course, is uncorrelated with the initial value, taking on a thermal distribution ( $dP/de = 2e$ ). Only for  $v_\infty > v_{\text{orb}}$  does the binary soften by a large amount—that is, if it is not destroyed completely, which is the overwhelmingly dominant outcome for this region of parameter space.

We have briefly explored the implications of our results. As mentioned above, the main implication is that the minimum size of a planetary system that will likely be destroyed as a result of dynamical interactions in dense stellar environments is larger than has been previously been assumed. For a stellar environment of a given velocity dispersion and density this limit can be read almost directly off of Figure 6. Applying our results to the observational campaigns searching for hot Jupiters in 47 Tuc via stellar transits, we find that the planetary systems that the Gilliland et al. (2000) observations were sensitive to would have in fact survived to the present day. This bolsters the conclusion drawn by Weldrake et al. (2005) that it is not dynamics that is responsible for the lack of hot Jupiters detected in 47 Tuc, but rather may be metallicity-dependent effects. Looking toward the future, we predict a MSP–planet binary may likely be detected via pulsar timing in the super-solar metallicity cluster Terzan 5, with a semi-major axis of  $\sim 0.1$  AU.

Recognizing that the planetary system PSR B1620-26 in the globular cluster M4 lies in the “intermediate” region of parameter space, we have performed a detailed numerical study of the possible scenarios in which it may have formed. By calculating cross sections and interaction rates, and treating the effects of mass transfer in the inner binary, we conclude that the scenario in which a NS–MS binary exchanges as a single dynamical unit into the planetary system for the planet’s original host star (similar to the scenario of Ford et al. 2000), is strongly favored over that of Sigurdsson et al. (2003), in which the exchange interaction involves ejecting the original NS binary companion, with the planet’s host star exchanging into it. This statement is quantified in Figure 8 for a wide range of initial binary semimajor axes.

Our general analysis (sections 2 through 5) does not consider the effects of direct physical collisions between objects (e.g., MS stars and planets), which may play an important role when the ratio of stellar size to binary semimajor axis is  $\gtrsim 0.01$  (Fregeau et al. 2004). However, our code accurately treats physical collisions, and we have allowed for collisions in our analysis of PSR B1620-26 in section 6, as shown in the cross sections of Figure 7. We have not looked at the ejection speeds of the planets in encounters which destroy the planetary system. This topic has already been studied in detail using  $N$ -body methods (Smith & Bonnell 2001; Hurley & Shara 2002).

Since our results assume point-mass particles, they are applicable to systems of any mass, as long as the mass ratio in the binary is relatively small  $\lesssim 0.1$ , and the incoming object and the heaviest object in the binary are of comparable mass. We have not yet explored the application to scenarios involving, e.g., intermediate-mass black holes and super-massive black holes, stars and intermediate-mass black holes, and planetesimals and planets. Our results may also have limited application to wide mass ratio binaries containing more than

one light body, as long as the total mass in light objects is significantly less than the host mass, and the orbits of the light objects are not so strongly coupled that they transmit perturbations on timescales comparable to the orbital period.

It is a pleasure to thank Natasha Ivanova for infor-

mative discussions about mass transfer in binaries. We also thank the anonymous referee for many helpful comments on the manuscript. This work was supported by NSF grants AST-0206182 and AST-0507727, and NASA grant NAG5-12044.

#### REFERENCES

- Backer, D. C. 1993, in ASP Conf. Ser. 36: Planets Around Pulsars, 11–18
- Basri, G. 2004, *Nature*, 430, 24
- Beer, M. E., King, A. R., & Pringle, J. E. 2004, *MNRAS*, 355, 1244
- Bonnell, I. A., Smith, K. W., Davies, M. B., & Horne, K. 2001, *MNRAS*, 322, 859
- Butler, R. P., Vogt, S. S., Marcy, G. W., Fischer, D. A., Henry, G. W., & Apps, K. 2000, *ApJ*, 545, 504
- Davies, M. B. & Sigurdsson, S. 2001, *MNRAS*, 324, 612
- Fischer, D. A. & Valenti, J. 2005, *ApJ*, 622, 1102
- Ford, E. B., Joshi, K. J., Rasio, F. A., & Zbarsky, B. 2000, *ApJ*, 528, 336
- Fregeau, J. M., Cheung, P., Portegies Zwart, S. F., & Rasio, F. A. 2004, *MNRAS*, 352, 1
- Gehrels, N. 1986, *ApJ*, 303, 336
- Gilliland, R. L., Brown, T. M., Guhathakurta, P., Sarajedini, A., Milone, E. F., Albrow, M. D., Baliber, N. R., Bruntt, H., Burrows, A., Charbonneau, D., Choi, P., Cochran, W. D., Edmonds, P. D., Frandsen, S., Howell, J. H., Lin, D. N. C., Marcy, G. W., Mayor, M., Naef, D., Sigurdsson, S., Stagg, C. R., Vandenberg, D. A., Vogt, S. S., & Williams, M. D. 2000, *ApJ*, 545, L47
- Harris, W. E. 1996, *AJ*, 112, 1487
- Heggie, D. & Hut, P. 2003, *The Gravitational Million-Body Problem: A Multidisciplinary Approach to Star Cluster Dynamics* (Cambridge University Press, 2003, 372 pp.)
- Heggie, D. C. 1975, *MNRAS*, 173, 729
- Heggie, D. C., Hut, P., & McMillan, S. L. W. 1996, *ApJ*, 467, 359
- Hills, J. G. 1975, *AJ*, 80, 809
- . 1984, *AJ*, 89, 1559
- . 1990, *AJ*, 99, 979
- Hills, J. G. & Dissly, R. W. 1989, *AJ*, 98, 1069
- Hurley, J. R. & Shara, M. M. 2002, *ApJ*, 565, 1251
- Hut, P. 1983, *ApJ*, 268, 342
- Hut, P. & Bahcall, J. N. 1983, *ApJ*, 268, 319
- Kenyon, S. J. & Bromley, B. C. 2004, *Nature*, 432, 598
- Kobayashi, H., Ida, S., & Tanaka, H. 2005, *Icarus*, 177, 246
- Konacki, M. 2005, *Nature*, 436, 230
- Laughlin, G. & Adams, F. C. 1998, *ApJ*, 508, L171
- McMillan, S. L. W. & Hut, P. 1996, *ApJ*, 467, 348
- Morbidelli, A. & Levison, H. F. 2004, *AJ*, 128, 2564
- Pfahl, E. 2005, *ApJ*, submitted (astro-ph/0509490)
- Podsiadlowski, P., Rappaport, S., & Pfahl, E. D. 2002, *ApJ*, 565, 1107
- Portegies Zwart, S. & McMillan, S. 2005, *ApJ*, in press (astro-ph/0509767)
- Portegies Zwart, S. F., McMillan, S. L. W., Hut, P., & Makino, J. 2001, *MNRAS*, 321, 199
- Ransom, S. M., Hessels, J. W. T., Stairs, I. H., Freire, P. C. C., Camilo, F., Kaspi, V. M., & Kaplan, D. L. 2005, *Science*, 307, 892
- Rasio, F. A., Shapiro, S. L., & Teukolsky, S. A. 1992, *A&A*, 256, L35
- Sigurdsson, S. 1992, *ApJ*, 399, L95
- Sigurdsson, S., Richer, H. B., Hansen, B. M., Stairs, I. H., & Thorsett, S. E. 2003, *Science*, 301, 193
- Sigurdsson, S. & Thorsett, S. E. 2004, *ASP Conference Series*, TBD, TBD
- Smith, K. W. & Bonnell, I. A. 2001, *MNRAS*, 322, L1
- Thorsett, S. E., Arzoumanian, Z., Camilo, F., & Lyne, A. G. 1999, *ApJ*, 523, 763
- Weldrake, D. T. F., Sackett, P. D., Bridges, T. J., & Freeman, K. C. 2005, *ApJ*, 620, 1043